Article

Remote Atmospheric-Pressure Plasma Activation of the Surfaces of Polyethylene Terephthalate and Polyethylene Naphthalate

E. Gonzalez II, M. D. Barankin, P. C. Guschl, and R. F. Hicks

Langmuir, **2008**, 24 (21), 12636-12643• DOI: 10.1021/la802296c • Publication Date (Web): 04 October 2008

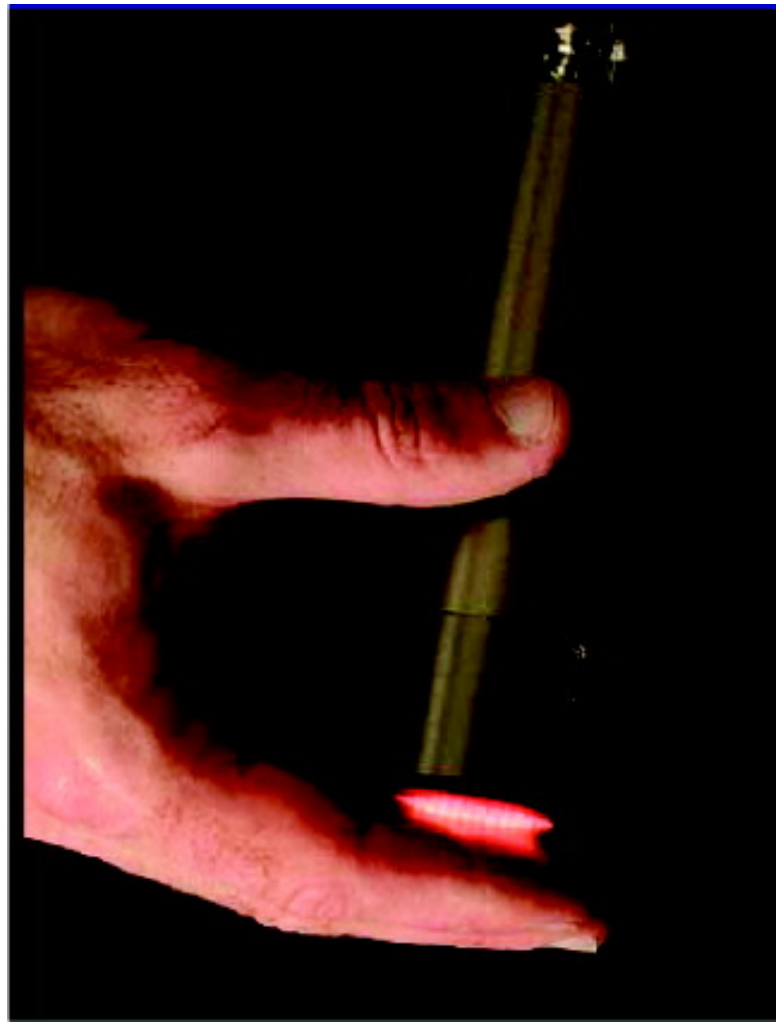

Remote Atmospheric-Pressure Plasma Activation of the Surfaces of Polyethylene Terephthalate and Polyethylene Naphthalate

E. Gonzalez II,[†] M. D. Barankin,[†] P. C. Guschl,[‡] and R. F. Hicks*,[†]

Department of Chemical and Biomolecular Engineering, University of California, Los Angeles, Los Angeles, California 90095, and Surfx Technologies LLC, 3617 Hayden Avenue, Culver City, California 90232

Received July 17, 2008. Revised Manuscript Received September 11, 2008

The surfaces of poly(ethylene terephthalate) (PET) and poly(ethylene naphthalate) (PEN) were treated with an atmospheric-pressure oxygen and helium plasma. Changes in the energy, adhesion, and chemical composition of the surfaces were determined by contact angle measurements, mechanical pull tests, and X-ray photoelectron spectroscopy (XPS). Surface-energy calculations revealed that after plasma treatment the polarity of PET and PEN increased 6 and 10 times, respectively. In addition, adhesive bond strengths were enhanced by up to 7 times. For PET and PEN, XPS revealed an 18−29% decrease in the area of the C 1s peak at 285 eV, which is attributable to the aromatic carbon atoms. The C 1s peak area due to ester carbon atoms increased by 11 and 24% for PET and PEN, respectively, while the C 1s peak area resulting from C−O species increased by about 5% for both polymers. These results indicate that oxygen atoms generated in the plasma rapidly oxidize the aromatic rings on the polymer chains. The Langmuir adsorption rate constants for oxidizing the polymer surfaces were 15.6 and 4.6 s^{-1} for PET and PEN, respectively.

Introduction

Low-temperature, atmospheric-pressure plasmas are emerging as important tools for the surface treatment of materials.[1−20] In particular, treating polymers with air or oxygen-containing atmospheric plasmas can raise their surface energy such that glues, inks, or coatings adhere more strongly to their surfaces. Vacuum plasmas are also suitable for modifying polymer surfaces.[21−28] However, a disadvantage of the latter equipment is that the work piece needs to be placed inside a chamber, which limits the size and shape of the object and adds to the overall process cost.

In spite of the inherent advantages of atmospheric pressure plasmas for treating polymer surfaces, few studies have investigated the mechanism and kinetics of this process.[1,3] The way that these sources treat materials is unique in that a beam of reactive species is produced that scans across the surface. The surface undergoes a dynamic change with time that depends on the density of radicals in the beam, the beam size, and the scan rate. Furthermore, the material may be placed downstream of the plasma and subjected nearly exclusively to neutral radical species. This may be contrasted to vacuum plasma treatment, where the substrate is placed between the electrodes and subjected to ion bombardment as well as to radical chemistry. Thus, we should expect the mechanism of polymer surface modification by atmospheric plasma to be fundamentally different from that in a low-pressure discharge.

In this paper, we report on the kinetics and mechanism of the activation of poly(ethylene terephthalate) (PET) and poly(ethylene naphthalate) (PEN) with a low-temperature, atmospheric-pressure helium and oxygen plasma. The polymers PET and PEN were chosen for this study because their chemical structures differ only in the number of aromatic carbon atoms available for plasma activation. The samples are placed downstream of the beam, where they are exposed primarily to ground-state oxygen

* To whom correspondence should be addressed.
[†] University of California, Los Angeles.
[‡] Surfx Technologies LLC.

(1) Hwang, Y. J.; Matthews, S.; McCord, M.; Bourham, M. *J. Electrochem. Soc.* **2004**, *151*(7), C495–C501.
(2) Schütze, A.; Jeong, J. Y.; Babayan, S. E.; Park, J.; Selwyn, G. S.; Hicks, R. F. *IEEE Trans. Plasma Sci.* **1998**, *26*, 1685–1694.
(3) Sladek, R. E. J.; Baede, T. A.; Stoffels, E. *IEEE Trans. Plasma Sci.* **2006**, (4), 34.
(4) Shenton, M. J.; Stevens, G. C. *J. Phys. D: Appl. Phys.* **2001**, *34*, 2761–2768.
(5) Foest, R.; Kindel, E.; Ohl, A.; Stieber, M.; Weltmann, K. D. *Plasma Phys. Controlled Fusion* **2005**, *47*, B525–B536.
(6) Villermet, A.; Cocolios, P.; Rames-Langlade, G.; Coeuret, F.; Gelot, J.; Prinz, E.; Forster, F. *Surf. Coat. Technol.* **2003**, *174−175*, 899–901.
(7) Akishev, Y.; Grushin, M.; Napartovich, A.; Trushkin, N. *Plasmas Polymers* **2002**, *7* (No. 3, Sept), 3, 261–289.
(8) Thurston, R. M.; Clayy, J. D.; Schulte, M. D. *J. Plast. Film Sheeting* **2007**, *23*, 63–78.
(9) Yang, S.; Gupta, M. C. *Surf. Coat. Technol.* **2004**, *187*, 172–176.
(10) Han, M. H.; Jegal, J. P.; Park, K. W.; Choi, J. H.; Baik, H. K.; Noh, J. H.; Song, K. M.; Lim, Y. S. *Surf. Coat. Technol.* **2007**, *201*, 4948–4952.
(11) Kuwabara, A.; Kuroda, S.; Kubota, H. *Plasma Sci. Technol.* **2007**, *9*(2), 181–189.
(12) Temmerman, E.; Akishev, Y.; Trushkin, N.; Leys, C.; Verschuren, J. *J. Phys. D: Appl. Phys.* **2005**, *38*, 505–509.
(13) Guimond, S.; Wertheimer, M. R. *J. Appl. Polym. Sci.* **2004**, *94*, 1291–1303.
(14) Barankova, H.; Bardos, L. *Surf. Coat. Technol.* **2003**) , *174 −175*, 63–67.
(15) Shenton, M. J.; Lovell-Hoare, M. C.; Stevens, G. C. *J. Phys. D: Appl. Phys.* **2001**, *34*, 2754–2760.
(16) Zhi, F.; Yuchang, Q.; Hui, W. *Plasma Sci. Technol.* **2004**, *6*(6), 2576–2580.
(17) Park, S. J.; Lee, H. W. *J. Colloid Interface Sci.* **2005**, *285*, 267–272.
(18) Yang, S.; Yin, H. *Plasma Chem. Plasma Process.* **2007**, *27*, 23–33.
(19) Jeong, J. Y.; Park, J.; Henins, I.; Babayan, S. E.; Tu, V. J.; Selwyn, G. S.; Ding, G.; Hicks, R. F. *J. Phys. Chem. A* **2000**, *104*, 8027–8032.
(20) Tynan, J.; Dowling, D. P.; Byrne, G.; Hughes, D. *Int. J. Nanomanufact.* **2007**, *1*, 554–569.
(21) Lim, H.; Lee, Y.; Han, S.; Cho, J.; Kim, K. *J. Vac. Sci. Technol. A* **2001**, *19*, 4.
(22) Duca, M. D.; Plosceanu, C. L.; Pop, T. *Polym. Degrad. Stab.* **1998**, *61*, 65–72.
(23) Grace, J. M.; Zhuang, H. K.; Gerenser, D. R.; Freeman, D. R. *J. Vac. Sci. Technol. A* **2003**, *21*, 1.
(24) Schulz, U.; Munzert, P.; Kaiser, N. *Surf. Coat. Technol.* **2001**, *142−144*, 507–511.
(25) Kitova, S.; Minchev, M.; Danev, G. *J. Optoelectron. Adv. Mater.* **2005**, *7*(1), 249–252.
(26) Hook, T. J.; Gardella, J. A., Jr. *J. Mater. Res.* **1987**, *2*, 1.
(27) Vargo, T. M.; Gardella, J. A.; Salvati, L., Jr. *J. Polym. Sci.: Part A: Polym. Chem.* **1989**, *27*, 1267–1286.
(28) Selli, E.; Mazzone, G.; Oliva, C.; Martín, F.; Riccardi, C.; Barni, R.; Marcandalli, B.; Massafra, M. R. *J. Mater. Chem.* **2001**, *11*, 1985–1991.

10.1021/la802296c CCC: $40.75
Published on Web 10/04/2008

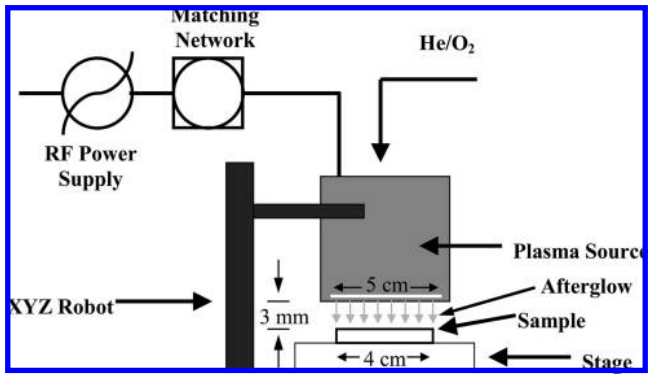

Figure 1. Schematic of the linear plasma source.

atoms.[19] Measurements are taken of the dynamic change in the water contact angle and surface energy with time and are shown to fit a Langmuir adsorption mechanism. Adhesive pull tests have been performed to demonstrate the connection between surface chemical modification and adhesive bond strength. Finally, the surfaces are analyzed by X-ray photoelectron spectroscopy (XPS) in order to discern the mechanism of surface activation.

Experimental Methods

Plasma Treatment. The plasma system used in these experiments was an Atomflo 350 L from Surfx Technologies LLC. A schematic of the apparatus is shown in Figure 1. It was connected to a gas supply and a radio-frequency (RF) power generator with a matching network operating at 27.12 MHz. Unless noted otherwise, the plasma was fed with 0.8 L/min of ultrahigh-purity oxygen and 30.0 L/min of helium at 1 atm and an RF power of 150 W. A 5 cm beam of reactive gas species flowed out of the end of the source. An XYZ robot, RB300-XY from Surfx Technologies LLC, was used to translate the plasma source over the materials. The source was affixed to an aluminum stage at a "standoff distance" of 3 mm from the surface of the substrate, and a scan speed of 250 mm/s was used. Samples were stored in a plastic container and covered to prevent dust accumulation.

A series of experiments were performed to estimate the plasma exposure time. First, a substrate was cleaned using the same procedure as that described in the Materials section. Next, the plasma was ignited and placed approximately 10 cm above the substrate. Using the robot, the plasma source was dropped down toward the substrate at 250 mm/s until a source-to-substrate separation of 3 mm was obtained. The substrate was treated for 2 s, and then the plasma source was moved away at 250 mm/s. Water contact angle measurements were taken perpendicularly to the treated area. The change in the water contact angle was plotted versus the position, and a Lorentzian curve was obtained. The area under the curve was integrated, and its value was divided by half of the maximum peak height, in order to obtain L, the effective plasma beam width. The value of L was calculated to be 2.1 cm. The exposure time was calculated by dividing L by the scan speed and multiplying by the number of scans.

Materials. PET (Ertalyte PET-P), with a thickness of 0.64 cm, was obtained from Boedecker Plastics Inc., and PEN, 0.1 mm thick, was received from DaiNippon Printing Co. Large sheets of these polymers were cut into 4 × 4 cm^2 squares and cleaned with commercial isopropyl alcohol. The squares were then baked on a digital hot plate at 60 °C to remove any remaining solvent or water from the surface prior to plasma treatment. For the aging experiments, the treated samples were stored in plastic containers and covered.

Surface Characterization. Contact angles of test liquids were recorded using a Krüss EasyDrop goniometer. The liquids tested were distilled water, glycerol, and diiodomethane. Approximately 10 droplets, 2 μL in volume, were measured on each sample's surface, and a software program quickly measured the contact angles. For each sample, the mean and standard deviation were calculated. Using the Owens, Wendt, Rabel, and Kaelble method, surface energy values were calculated as follows:[29]

$$\frac{(1+\cos\theta)\sigma_l}{2\sqrt{\sigma_l^D}} = \sqrt{\sigma_s^P}\sqrt{\frac{\sigma_l^P}{\sigma_l^D}} + \sqrt{\sigma_s^D} \quad (1)$$

θ is the static contact angle of the liquid on the surface of the polymer, σ_l is the surface energy of liquid, and σ_s is the surface energy of the polymer. Superscripts D and P represent the dispersive and polar components of the surface energy accordingly. It should be noted that the total surface energy of a liquid or solid is equal to the sum of the dispersive and polar components. The surface energy was calculated for the control samples, the plasma-treated samples immediately after exposure, and the plasma-treated samples aged for up to 4000 h in an ambient of 75 °F and 40% relative humidity.

The surface composition of the polymers was analyzed by XPS before and after plasma treatment. Core-level photoemission spectra of the C 1s and O 1s lines were collected with a PHI 3057 spectrometer using Mg Kα X-rays at 1286.6 eV. All XPS spectra were taken in small-area mode with a 7° acceptance angle and 23.5 eV pass energy. The detection angle with respect to the surface normal was 25°. All spectra were referenced to the C 1s peak of the graphitic carbon atom, with an assigned value of 285.0 eV. The surface atomic percentages were determined from the integrated intensity of the C 1s and O 1s photoemission peaks, divided by their sensitivity factors, 0.30 and 0.71, respectively.[30]

Adhesion Testing. The pull strengths of adhesives to PET were measured using mechanical pull tests according to ASTM D4541. The apparatus was a PosiTest Pull-Off Adhesion Tester from DeFelsko Corp. The adhesives were as follows: Hardman, Inc., epoxy (04005); Hardman, Inc., D-50 urethane (04022); NuSil Technology medical-grade silicone adhesive (MED1-4013); 3 M Scotch-Weld acrylic adhesive (DP 805). The PET was cut into 1.5 × 8 $in.^2$ strips and plasma-treated using two different conditions: (1) a "short plasma" treatment consisting of 0.8 L/min of oxygen, 30.0 L/min of helium, a 3 mm standoff distance, 150 W of RF power, a 70 mm/s scan speed, and 4 total scans and (2) a "long plasma" treatment consisting of 0.9 L/min of oxygen, 30.0 L/min of helium, a 5 mm standoff distance, 200 W of RF power, a 10 mm/s scan speed, and 16 total scans. Also, for the "long plasma" case, the aluminum dollies were scanned once with the plasma at 50 mm/s in order to improve the adhesive bond at that interface. Immediately after treatment, five aluminum dollies, 20 mm in diameter, were bonded to the PET surfaces. Approximately 1% glass beads (150−200 μm diameter) were mixed into the adhesive to control the bond-line thickness. The bonded dollies were allowed to cure for at least 24 h before they were tested. For adhesion testing, the actuator was placed on top of the dolly and the sample was primed by pushing the hydraulic pump until 100 psi was reached. Once primed, a pull rate between 100 and 150 psi/s was maintained until the dollies broke off the plastic.

Rinsing. Two PET samples were treated simultaneously using a plasma fed with 0.5 L/min of ultrahigh-purity oxygen and 30.0 L/min of helium at 1 atm and an RF power of 120 W. A total of four scans were performed at 70 mm/s. Then one sample was rinsed with methanol and allowed to dry at room temperature for about 16 h. After the drying period ended, XPS spectra were obtained for both samples.

Results

Plasma Exposure Time. Figure 2 shows the dependence of the water contact angle on the distance from the beam center after plasma exposure. The data points were fitted with a Lorentzian curve, and the area under the curve was calculated to be 249.4 ° mm. This area was divided by half of the maximum

(29) Kaelble, D. H. *J. Adhesion* **1970**, *2*, 66.
(30) Physical Electronics Inc., PHI Reference Tables.

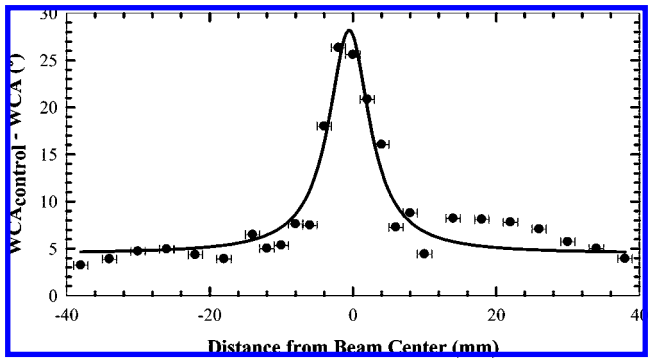

Figure 2. Dependence of the water contact angle on the distance from the beam center after plasma exposure.

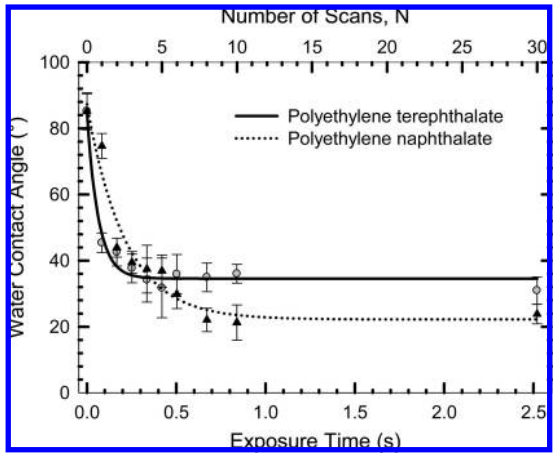

Figure 3. Dependence of the water contact angles of PET and PEN on the plasma exposure time.

peak height (11.9°) to yield a value of 21.0 mm for L, the effective beam width. The exposure time of the sample in the plasma equals the beam width divided by the scan rate (250 mm/s) times the number of scans: $\tau = 0.084N$ s.

Contact Angle and Surface Energy. The effect of the atmospheric plasma exposure time on the water contact angles of PET and PEN is shown in Figure 3. The samples were treated with 0.8 L/min of oxygen, 30.0 L/min of helium, 150 W, and a 3 mm standoff distance. The data points on the graph follow an exponential decay behavior typical for Langmuir adsorption kinetics.[31] This observation will be discussed later in the paper. The initial contact angle of PET was 85.2 ± 5.2°. It dropped to 35 ± 4.1° after about 0.25 s of plasma treatment. PEN manifested a greater drop in the water contact angle than PET: The initial contact angle was 85.2 ± 4.6°, and the minimum value was 20.5 ± 4.2° after 0.7 s of exposure.

The following equation was fitted to the contact angle data as a function of the exposure time, τ, of the following form:

$$\mathrm{WCA}(t) = \mathrm{WCA}(\infty) + [\mathrm{WCA}(0) - \mathrm{WCA}(\infty)] \exp(-k\tau) \quad (2)$$

which can be rearranged to

$$\frac{\mathrm{WCA}(t) - \mathrm{WCA}(\infty)}{\mathrm{WCA}(0) - \mathrm{WCA}(\infty)} = \exp(-kt) \quad (3)$$

where WCA(∞) is the water contact angle after maximum plasma treatment, WCA(0) is the initial water contact angle, and k is the reaction rate constant. The equation parameters are listed in Table 1. Note that the rate constant for surface activation of PET is 3-fold higher than that for PEN.

Table 1. Parameters for the Exponential Decay Equation (2) Corresponding to PET and PEN

	WCA(0)	WCA(∞)	k (s^{-1})
PET	85.2	34.6	15.6
PEN	85.2	21.7	4.6

In order to assess the importance of reactive oxygen species for surface activation, PET was exposed to a helium plasma. The change in the water contact angle with the exposure time is compared to that achieved with the helium and oxygen plasma in Figure 4. The former discharge was operated with 30 L/min of industrial-grade helium, 120 W, a 3 mm standoff distance, and a scan speed of 250 mm/s. The helium/oxygen plasma used the same parameters, with the only difference being the addition of 0.5 L/min of oxygen. The initial water contact angle of PET was 83 ± 4.4°. After about 0.6 s of exposure to the helium plasma, the water contact angle of PET fell to 46 ± 5.1°. This may be compared to the helium/oxygen plasma, where only 0.08 s of exposure is needed for the contact angle to drop to 45 ± 2.4°. In Figure 4, the solid and dashed curves are the best fits of eq 3 to the data for the helium discharges with and without oxygen, respectively. From the fits, the rate constants for surface activation were found to be 1.4 s^{-1} for the helium plasma and 18.1 s^{-1} for the helium/oxygen plasma. The reactive oxygen species generated in the latter plasma greatly accelerate the surface reaction rate.

Because the source is being translated over the surface of the polymer using a robot, it is possible that oxygen present in the atmosphere may mix with the effluent of the helium plasma and become activated. Therefore, experiments using a single scan to activate PET were performed. These results are presented in Figure 5. The water contact angle changed by approximately 10° when the helium plasma was scanned over the surface at 10 mm/s. By contrast, WCA fell 60° when scanned at the same speed with the helium/oxygen plasma. Once again, it is confirmed that reactive oxygen species are primarily responsible for polymer surface activation.

Although the plasma has an immediate effect on the contact angle of the polymers, we wanted to determine how long this treatment lasts. Therefore, aging experiments were performed on the plasma-treated polymer samples, and the results are shown in Figure 6. The samples were scanned four times using a speed of 40 mm/s. It should be noted that this scan speed resulted in

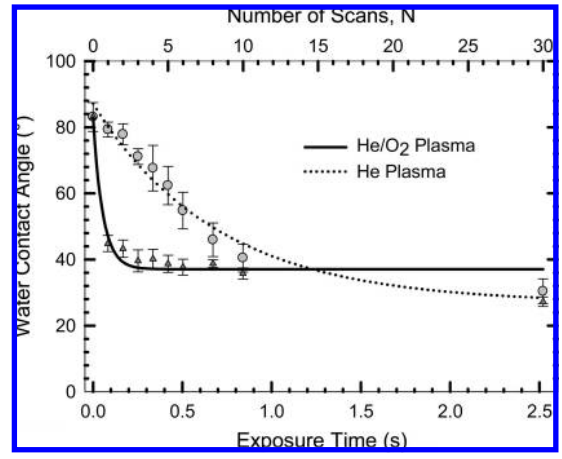

Figure 4. Dependence of the water contact angle of PET upon exposure to the helium and helium/oxygen plasmas.

(31) Fogler, H. S. *Elements of Chemical Reaction Engineering*; Prentice Hall PTR: Upper Saddle River, NJ, 1999.

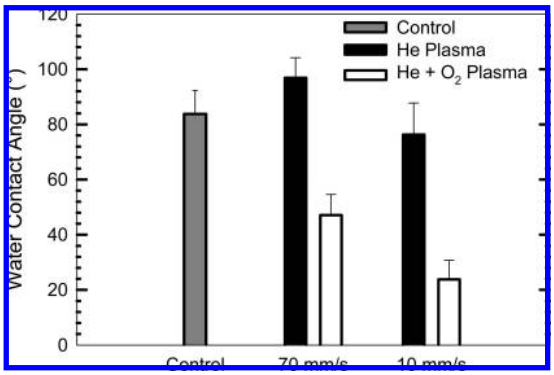

Figure 5. Dependence of the water contact angle of PET upon exposure to helium and helium/oxygen plasmas using a single scan at 70 and 10 mm/s.

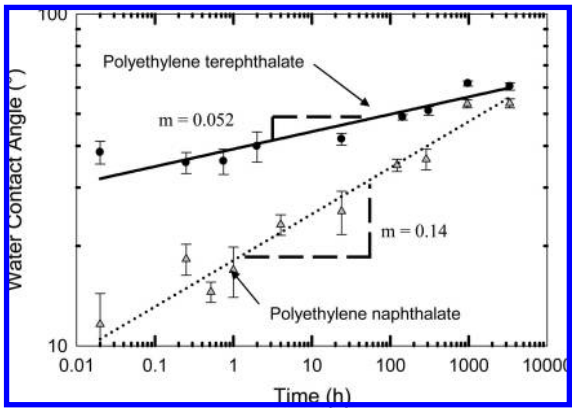

Figure 6. log−log plot of the change in the contact angle of surface-activated PET and PEN with time.

Table 2. Polymer Surface Energies before and after Plasma Treatment and Aging

polymer	experiment	surface energy (dyn/cm)	dispersive (dyn/cm)	polar (dyn/cm)	polarity (%)
PET	control	43.5	39.3	4.2	9.7
	plasma	55.4	30.9	24.5	44.3
	aged[a]	43.7	29.4	14.3	32.8
PEN	control	44.7	40.5	4.1	9.3
	plasma	64.9	25.7	39.2	60.4
	aged[a]	46.7	28.5	18.1	38.9

[a] Approximately 4000 h after plasma treatment.

a lower water contact angle when compared to the results in Figure 3. The plasma-treated PET had a starting contact angle value of 38 ± 3° and increased to about 61 ± 4° after 4000 h. This final value is approximately 20° less than the untreated value. The equation for the aging of PET was

$$\Delta\mathrm{WCA} = 39.2t^{0.052} \quad (4)$$

After plasma treatment, PEN had a contact angle of 12 ± 3°. After 4000 h, it rose to a value of 54 ± 2°, which is 30° less than the untreated value. The equation for the aging of PEN was

$$\Delta\mathrm{WCA} = 39.2t^{0.14} \quad (5)$$

Surface energies, along with their dispersive and polar components, are listed in Table 2. The surface energies of PET and PEN were calculated for the control, plasma-treated, and aged samples. The surface energy of PET increased from 43.5 to 55.4 dyn/cm after exposure to the atmospheric plasma. This was accompanied by a slight drop in the dispersive component

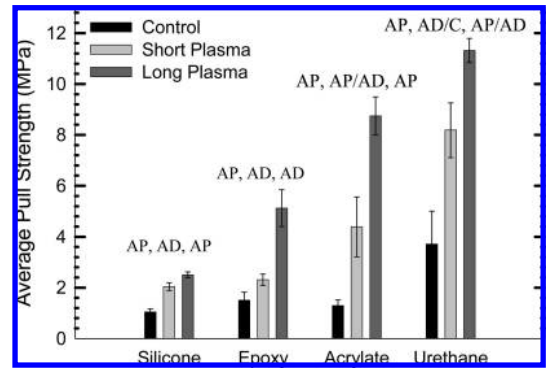

Figure 7. Effect of plasma treatment on the pull strength for adhesively bonded PET.

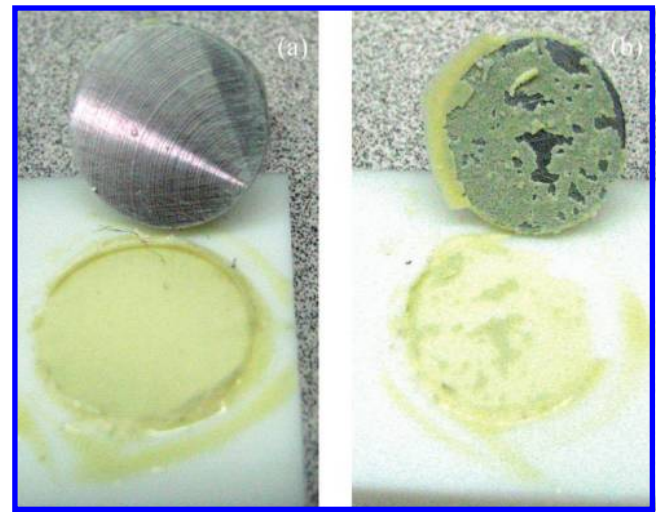

Figure 8. Image of PET samples bonded with urethane showing (left, a) adhesive failure at the adhesive/dolly interface and (right, b) cohesive failure.

and a 6-fold increase in the polar component. After 4000 h of aging, the surface energy dropped back down to the untreated value of 43.7 dyn/cm. Nevertheless, the nonpolar component of PET remained close to 30 dyn/cm, while the polar component was 14.3 dyn/cm, which was 3 times higher than its original value. A similar, but more dramatic, trend was seen with PEN. Its polar component increased by nearly 10-fold after plasma treatment. After 4000 h of aging, the surface energy dropped down close to the untreated value. On the other hand, the polar component of the aged PEN was 18.1 dyn/cm, which was almost 5 times higher than the untreated value.

Adhesive Bonding. Figure 7 shows the adhesive bonding results for PET. The letters "AD" in Figure 7 represent adhesive failure at the adhesive/dolly interface. An image of this type of failure can be seen in Figure 8a. The adhesive is completely bonded to the plastic, and the surface of the dolly is left without any adhesive. The letters "AP" represent adhesive failure at the adhesive/plastic interface, and they are characterized by the adhesive staying completely on the dolly with none on the plastic surface when the pull test is performed. The letter "C" represents cohesive failure in which the adhesive ruptures. As can be seen in Figure 8b, cohesive failure occurs when a layer of glue remains on both the dolly and the plastic.

The bond strength for all four adhesives was increased by plasma treatment. For the acrylate, the pull strength jumped by almost 7-fold, whereas for the epoxy and urethane, the pull strength was increased by more than 3-fold. The silicone pull

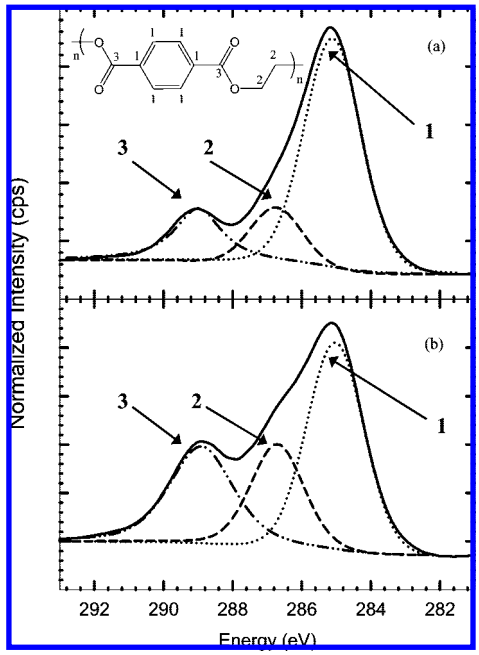

Figure 9. C 1s XPS spectra of (a) control PET and (b) plasma-treated PET.

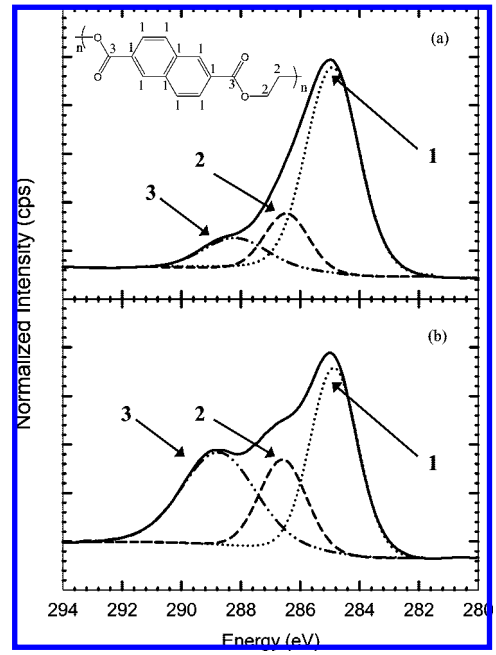

Figure 10. C 1s XPS spectra of (a) control PEN and (b) plasma-treated PEN.

strength increased by approximately 2.5 times. Note that all of the control specimens failed at the adhesive/plastic interface. For the "short plasma" samples, failure occurred at the adhesive/dolly interface for some, if not all, of the samples. Therefore, when the "long plasma" treatment samples were performed, the aluminum dollies were also treated prior to bonding. This resulted in failure at the plastic/adhesive interface for silicone and acrylate and both plastic/adhesive and dolly/adhesive failure for urethane. As for the epoxy, failure occurred at the dolly. Because of failure occurring at the adhesive/dolly interface, we cannot say how much the bond strength was improved for the epoxy.

XPS Analysis. For these measurements, samples were scanned four times at 40 mm/s with 0.8 L/min of oxygen, 30.0 L/min of helium, a 3 mm standoff distance, and a RF power of 150 W. The C 1s spectra of PET before and after plasma treatment are shown in Figure 9. Each spectrum was deconvoluted into three peaks, which are assigned as follows: (1) aromatic carbon atoms at 285.0 eV; (2) methylene carbon atoms at 286.6 eV; (3) ester carbon atoms at 289.0 eV (see the inset diagram in Figure 9). These assignments are consistent with previous studies of PET surfaces.[32] A comparison of the data before and after treatment reveals that the amount of aromatic carbon on the polymer surface decreases relative to the methylene and oxidized carbon atoms. Furthermore, it is important to note that no new C 1s peaks are observed at higher binding energies following plasma activation.

The C 1s spectra of PEN before and after plasma treatment are shown in Figure 10. The C 1s peak was deconvoluted into the same three peaks as are seen for PET, except in this case the number of aromatic carbon atoms (1) is proportionally larger. Once again, it is seen that after plasma treatment the amount of aromatic carbon decreases relative to the methylene and oxidized carbon atoms, and also no new C 1s peaks are observed.

Table 3 shows the C 1s binding energies and surface compositions of the polymers before and after plasma treatment. The C:O ratio of the control PET is 3.0. The atomic C:O ratio of the repeat unit for PET is 2.5. The difference between the observed C:O ratio and that of the repeat unit may be due to some carbon contamination on the surface of the polymer. After plasma treatment, the C:O ratio drops to 1.7. For the control sample, peak 1 accounts for approximately 70% of the total C 1s band area, whereas peaks 2 and 3 account for 14.3% and 17.7%, respectively. After plasma treatment, peak 1 decreases to 50.5% of the total C 1s area, while peaks 2 and 3 increase to 20.4% and 29.1%, respectively. The C:O ratio of the control PEN is 3.5. After plasma treatment, the C:O ratio drops to 1.8. For the control sample, peaks 1−3 account for 74, 14, and 12% of the total C 1s band area, respectively. After plasma treatment, peak 1 decreases to 45% of the total C 1s area, while peaks 2 and 3 increase to 19% and 36%, respectively. These results show that more C−O and C═O bonds are present on the surface of the polymers after exposure to the atmospheric-pressure oxygen and helium plasma.

Figure 11 shows the O 1s spectra for PET before and after plasma treatment. The peak was deconvoluted into two peaks. The first one, which is located at 532.3 eV, is attributed to C═O. The second peak, located at 533.8 eV, is attributed to C−O. The data reveal that the number of double bonds to oxygen increases equally as much as those of the single bonds. Additionally, no new O 1s peaks are observed after plasma activation. Similarly, the O 1s peak for PEN was deconvoluted into two peaks at 532.3 and 533.8 eV, as shown in Figure 12. Once more, the data show an equal increase in the amount of C═O relative to C−O.

The O 1s binding energies and surface compositions for the control and plasma-treated polymers are listed in Table 3. These data show that, for both PET and PEN, there is no changes in the distribution of C═O and C−O, with these species remaining at a 51:49 ratio to one another.

Table 4 shows the effect of a methanol rinse on the surface composition of the polymer after plasma treatment. The percentage of aromatic carbon atoms found at 285.0 eV increased from 49% to 56%, while the amount of carbon atoms associated with C−O bonds and ester groups dropped by 3 and 4%, respectively. In addition, the water contact angle increased from 41.4 ± 4.0° to 50.6 ± 7.0°. These results indicate that the plasma exposure may generate a small amount of low-molecular-weight (LMW)

(32) Boulanger, P.; Pireaux, J. J.; Verbist, J. J.; Delhalle, J. *J. Electron Spectrosc. Relat. Phenom.* **1993**, *63*, 53–73.

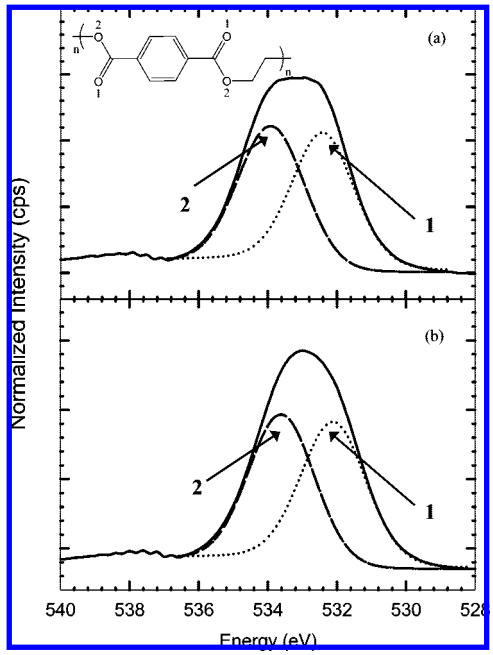

Figure 11. O 1s XPS spectra of (a) control PET and (b) plasma-treated PET.

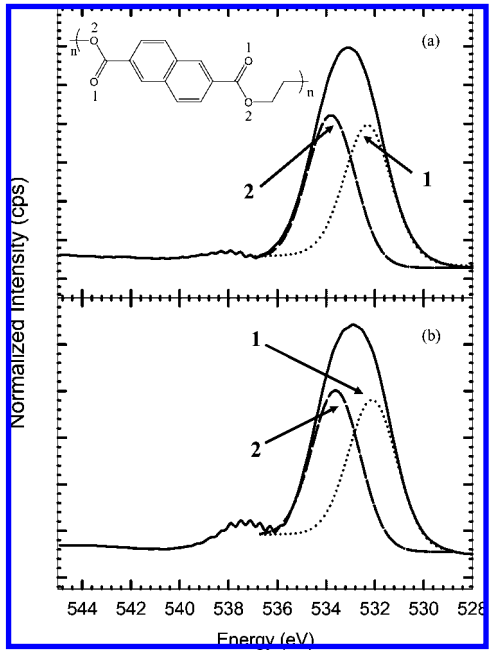

Figure 12. O 1s XPS spectra of (a) control PEN and (b) plasma-treated PEN.

polymer chains that are soluble in methanol.[11,13,15] Nevertheless, the surface energy and chemical composition of the activated PET are not changed that much by removal of the LMW species.

Discussion

Adsorption Kinetics. The effect of the plasma exposure time on the water contact angle of the polymers (cf. Figure 3) can be rationalized through a Langmuir adsorption model. The surfaces of the polymers have a fixed number of sites available for attack by the reactive atoms in the plasma. When the plasma is ignited, oxygen atoms are produced with a concentration of about 5×10^{15} cm^{-3}.[19] These diradicals travel toward the surface of the polymer and react with the available sites. A mass balance on the surface sites yields

$$[\mathrm{L}]\frac{\mathrm{d}[\theta_\mathrm{v}]}{\mathrm{d}t} = -k'[\mathrm{O}^\bullet]\theta_\mathrm{v} \tag{6}$$

where k' is the Langmuir adsorption rate constant, [O•] is the concentration of diradicals, [L] is the surface site density, and θ_v is the fraction of unreacted sites. This expression can be rearranged and solved to give

$$\theta_\mathrm{v} = \mathrm{e}^{-k'[\mathrm{O}^\bullet]t/[\mathrm{L}]} \tag{7}$$

The fraction of unreacted sites, θ_v, is related to the water contact angle of the polymer by the following expression:

$$\theta_\mathrm{v} = \frac{\mathrm{WCA}(t) - \mathrm{WCA}(\infty)}{\mathrm{WCA}(0) - \mathrm{WCA}(\infty)} \tag{8}$$

because at $t = 0$, WCA = WCA(0) and $\theta_\mathrm{v} = 1$, while at $t = \infty$, WCA = WCA(∞) and $\theta_\mathrm{v} = 0$. A comparison of these equations with eq 3 reveals that the rate constant, k, obtained from the water contact data equals the Langmuir adsorption rate constant, k', multiplied by the concentration of oxygen diradicals, [O•], and divided by the density of sites, [L].

Akishev et al. [7] treated several polymers with a low-temperature, atmospheric-pressure plasma and obtained curves for a change in the water contact angle with time that are similar to those shown in Figure 3. They did not attempt to relate the data to Langmuir adsorption kinetics. Herein, the surface activation rate constants were found to be 15.6 and 4.6 s^{-1} for PET and PEN. Although the rate constant for PET was about 3 times higher than that for PEN, the latter polymer saw a greater increase in polarity and ultimately a lower water contact angle. Perhaps the difference in the rate constants is due to the different density of sites on the two polymer surfaces, e.g., benzene versus naphthalene rings in the chains.

The polymer aging experiments shown in Figure 6 reveal that, after approximately 4000 h, the contact angles have not returned to their original values. The surface activation effect of the polymers seen in this study lasts much longer than that of other atmospheric plasmas.[9,18] Although the surface energies of the polymers have returned to their initial values, the polarities of the polymers have not, suggesting a permanent change in the polymer surfaces. According to Koh et al.,[33] the increase in the polarity for a polymer is mainly due to the formation of polar groups such as ether [−(C−O)−], carbonyl [−(C═O)−], ester [−(C═O)−O], hydroxyl [−(O−H)], and peroxide [−(C−O−OH)] bonds. For the control polymer samples, the dispersive component of the surface energy was much greater than the polar component. However, after plasma treatment, the polar component increased while the dispersive component decreased. The decrease in the dispersive component was still evident even after 4000 h of aging, suggesting an irreversible reaction of oxygen with the polymer chains, creating polar groups. The observed decrease in the polymer component of the surface energy with time may be due to the exchange of surface polar molecules with nonpolar molecules from the bulk material.

Rinsing the surface of PET with methanol after plasma treatment caused the amount of C−O bonds and ester-like carbons to decrease by about 4% each. The rinse removed any LMW degradation products resulting from the plasma treatment.[11,13,15] The amount of LMW species present on the surface is a small percentage of the total amount of species that have been oxidized on the surface. Also, it should be noted that the water contact angle did not return to its original value before plasma treatment, showing that the surface of the polymer has been altered. Although

(33) Koh, S. K.; Cho, J. S.; Kim, K. H.; Han, S.; Beag, Y. W. *J. Adhesion Sci. Technol.* **2002**, *16*(2), 129.

Table 3. C 1s and O 1s Binding Energies and Surface Compositions of the Polymers before and after Plasma Treatment

		control			plasma-treated		
	peak no.	binding energy (eV)	fraction of total elements (%)	C:O ratio	binding energy (eV)	fraction of total elements (%)	C:O ratio
				PET			
C 1s	1	285.0	68.0	3.0	285.0	50.5	1.7
	2	286.6	14.3		286.7	20.4	
	3	289.0	17.7		288.9	29.1	
O 1s	1	532.3	50.9		532.3	51.2	
	2	533.8	49.1		533.8	48.8	
				PEN			
C 1s	1	285.0	73.9	3.5	285.0	45.1	1.8
	2	286.6	14.1		286.6	19.2	
	3	288.9	12.0		288.9	35.6	
O 1s	1	532.3	51.0		532.3	50.8	
	2	533.8	49.0		533.8	49.2	

Table 4. Binding Energies, Surface Compositions, and Water Contact Angles of Plasma-Treated PET with and without Methanol Rinsing

		no rinsing				rinsing			
	peak no.	binding energy (eV)	fraction of total elements (%)	C:O ratio	WCA (deg)	binding energy (eV)	fraction of total elements (%)	C:O ratio	WCA (deg)
					PET				
C 1s	1	285.0	48.5	1.6	41.4 ± 4	285.0	55.6	1.8	50.6 ± 7
	2	286.7	22.6			286.7	19.4		
	3	288.9	29.0			288.9	25.1		
O 1s	1	532.3	51.5			532.3	56.8		
	2	533.8	48.5			533.8	43.2		

the XPS data shown in the remaining experiments may not be representative of the pure modified PET and PEN surfaces, they do show the general trend of plasma activation of both polymers.

Adhesion. The ASTM pull tests demonstrate that treating PET with the atmospheric helium and oxygen plasma increases the bond strength by 7-fold using the acrylate adhesive and by approximately 3-fold using the other adhesives. Tynan et al.[20] obtained analogous results for bonding of PET with the epoxy after exposure to an atmospheric helium and oxygen plasma. However, their system used much higher applied powers (900 W) than those in this work. Thurston et al.[8] used the same type of atmospheric pressure helium and oxygen plasma as that described herein. They reported an increase in the adhesion of polystyrene to silicone and epoxy of 3 and 4 times, respectively. Polystyrene is similar to PET and PEN in that it contains aromatic groups that may be attacked by the oxygen plasma. In another study, PET was treated with atmospheric-pressure air and nitrogen plasmas, and the bond strength to an epoxy adhesive was raised up to 10-fold.[15]

Mechanism of Surface Activation. Returning to the X-ray photoemission data presented in Table 3, we found that the C 1s peak corresponding to the aromatic carbons decreased significantly, while the C 1s peaks for the C−O and carbonyl bonds increased. In PET, the aromatic carbons account for 68% of the total carbon prior to treatment and 51% afterward. Conversely, the fraction of the carbon due to ester groups increased from 18 to 29%. PEN, which has 10 aromatic carbon atoms per unit compared to 6 for PET, saw its fraction of aromatic carbon drop from 74 to 45% after plasma exposure, while the fraction of the carbon due to ester groups rose from 12 to 36%. These data indicate that the aromatic ring is attacked by the oxygen atoms in the plasma and converted to "ester-like" species. Because PEN has more aromatic carbons present in its structure as compared to PET, the plasma is able to create more ester groups on the surface of PEN than of PET.

To account for the change in the composition of the polymers, a surface activation mechanism is proposed in Figure 13. The reaction is initiated by hydrogen abstraction from the methylene groups with the oxygen diradicals.[34−36] Note that the oxygen atoms are generated in high concentration in the plasma and are several orders of magnitude higher than ozone or metastable $O_2(^1\Delta_g)$.[19] The bond strength of the hydrogen to the aliphatic carbon is less than that of hydrogen to the aromatic carbon, which makes the methylene group the most likely site for hydrogen abstraction. The next step, reaction 2, is oxygen addition to the hydrocarbon radical on the polymer chain.[34,35] In the atmospheric plasma, the concentration of oxygen molecules is on the order of 10^{17} cm^{-3}[19] and is the most abundant species in the gas. In reaction 3, the polymer chain cleaves to form two carboxylic radicals.[34] As seen in reactions 4a and 4b, the two newly formed radicals can either create more radicals by the removal of CO_2[1,34,35,37] or form a carboxylic acid by the addition of hydrogen. In reaction 5, oxygenis added to the benzyl radical to create a peroxy radical,[38] which can decompose to a hydroxyl group as shown in reaction 6.[37,38]

The mechanism shown in Figure 13 can at least partially account for the increase in the C and O 1s peaks attributable to the C−O and C═O ester groups. However, if reactions 1−4 were the sole source of ester carbon atoms, then the increase in this feature in the XPS spectrum should be the same for both PET and PEN because both polymers have the same number of methylene groups per monomer unit. Nevertheless, our data show that more ester carbon atoms were created for PEN than for PET. Therefore, we suggest that the reaction mechanism proceeds further than the sequence of steps presented in Figure 13. Specifically, opening of the aromatic ring appears to be the only way to add additional ester groups to the polymer chain. This phenomenon was proposed previously by Callahan et al.[35] for

(34) Gheorghiu, M.; Arefi, F.; Amouroux, J.; Placinta, G.; Popa, G.; Tatoulian, M. *Plasma Sources Sci. Technol.* **1997**, *6*, 8–19.
(35) Callahan, R. R., A.; Raupp, G. B.; Beaudoin, S. P. *J. Vac. Sci. Technol. B* **2001**, (3), 19.
(36) Kumagai, H.; Hiroki, D.; Fujii, N.; Kobayashi, T. *J. Vac. Sci. Technol. A* **2004**, (1), 22.
(37) Inagaki, N.; Narushima, K.; Lim, S. K. *J. Appl. Polym. Sci.* **2003**, *89*, 96–103.
(38) Hansen, R. H.; Pascale, J. V.; De Benedictis, T.; Rentzepis, P. M. *J. Polym. Sci.: Part A* **2005**, *3*, 2205–2214.

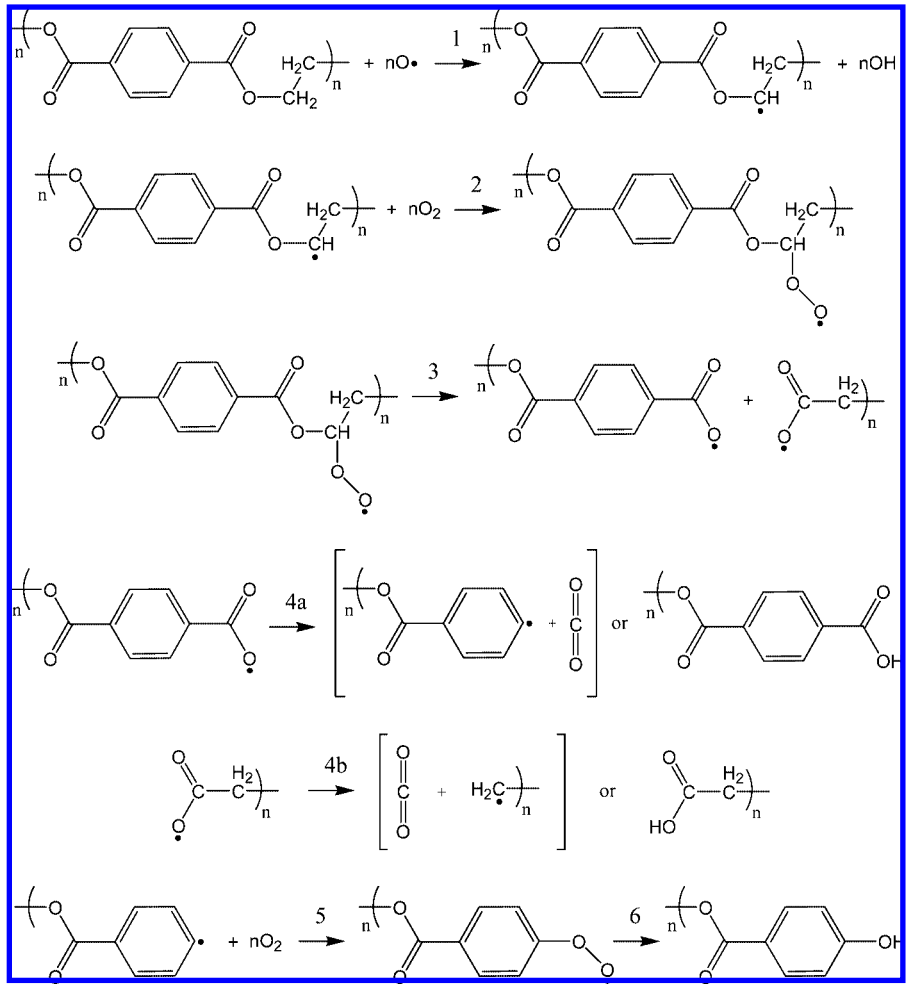

Figure 13. Proposed surface activation mechanism for PET.

the oxygen plasma treatment of parylene-N, which also contains backbone aromatic rings. Also, Selli et al.[28] reported the attack of the aromatic rings in PET after treatment with a vacuum SF_6 plasma. Experiments are currently being conducted in our laboratory with other aromatic polymers to further validate this claim.

Conclusions

The effect of atmospheric plasma activation of PET and PEN surfaces was investigated. PET saw a 50° drop in the water contact angle and a 6-fold increase in polarity after plasma treatment, while PEN experienced a 65° decrease in the water contact angle and a 10-fold increase in polarity. The effect of the plasma was still evident after 5 months of aging. The change in the surface energy after atmospheric plasma treatment of PET resulted in enhanced adhesive bonding. For the acrylate, the pull strength rose by 7-fold, while the pull strength for epoxy, urethane, and silicone rose by approximately 3-fold. The change in the surface properties of the polymers was due to the attack of the methylene and aromatic carbon atoms by oxygen radicals, with the formation of ester-like C−O and C═O bonds.

Acknowledgment. This research was done while under the appointment of a Department of Homeland Security fellowship. This research was supported by Plant Directed Research and Development funding from the Department of Energy's National Nuclear Security Administration's Kansas City Plant. The authors thank Dr. Robin L. Garrell from the UCLA Chemistry Department for her guidance and discussion.

LA802296C